Prognostic value and immune infiltration of ARMC10 in pancreatic adenocarcinoma via integrated bioinformatics analyses

Tian-Hao Li [a,1], Xiao-Han Qin [c,1], Li-Quan Wang [a,1], Cheng Qin [b], Bang-Bo Zhao [b], Hong-Tao Cao [b], Xiao-Ying Yang [b], Yuan-Yang Wang [b], Ze-Ru Li [b], Xing-Tong Zhou [a], Wei-Bin Wang [b,*]

[a] Department of Surgery, State Key Laboratory of Complex Severe and Rare Diseases, Peking Union Medical College Hospital, Chinese Academy of Medical Sciences, Peking Union Medical College, Beijing, China
[b] Department of General Surgery, Peking Union Medical College Hospital, Chinese Academy of Medical Sciences, Peking Union Medical College, Beijing, China
[c] Department of Cardiology, Peking Union Medical College Hospital, Chinese Academy of Medical Sciences, Peking Union Medical College, Beijing, China

ARTICLE INFO

ABSTRACT

Background: Armadillo repeat-containing 10 (ARMC10) is involved in the progression of multiple types of tumors. Pancreatic adenocarcinoma (PAAD) is a lethal disease with poor survival and prognosis.

Methods: We acquired the data of ARMC10 in PAAD patients from the cancer genome atlas (TCGA) and gene expression omnibus (GEO) datasets and compared the expression level with normal pancreatic tissues. We evaluated the relevance between ARMC10 expression and clinicopathological factors, immune infiltration degree and prognosis in PAAD.

Results: High expression of ARMC10 was relevant to T stage, M stage, pathologic stage, histologic grade, residual tumor, primary therapy outcome (P < 0.05) and related to lower Overall-Survival (OS), Disease-Specific Survival (DSS), and Progression-Free Interval (PFI). Gene set enrichment analysis showed that ARMC10 was related to methylation in neural precursor cells (NPC), G alpha (i) signaling events, APC targets, energy metabolism, potassium channels and IL10 synthesis. The expression level of ARMC10 was positively related to the abundance of T helper cells and negatively to that of plasmacytoid dendritic cells (pDCs). Knocking down of ARMC10 could lead to lower proliferation, invasion, migration ability and colony formation rate of PAAD cells in vitro.

Conclusions: Our research firstly discovered ARMC10 as a novel prognostic biomarker for PAAD patients and played a crucial role in immune regulation in PAAD.

1. Background

Pancreatic cancer is one of the most lethal malignant tumors with the lowest 5-year relative survival rate of 11% [1]. Pancreatic

---

* Corresponding author.
  E-mail address: wwb_xh@163.com (W.-B. Wang).
[1] Tian-Hao Li, Xiao-Han Qin and Li-Quan Wang contributed equally to this work.

adenocarcinoma (PAAD) is the most prevalent type of pancreatic cancer [2]. Albeit exploring for a long time, there is still few satisfactory results on early prognosis and therapy of PAAD, and most patients suffer from PAAD still present with surgically unresectable and widespread metastasis [1,3–5]. In recent years, various biomarkers have been uncovered to promote or inhibit the procession of pancreatic cancer on molecular levels, such as miRNA [6–8], lncRNA [9–11], circRNA [12–14] and protein [15–17]. However, neither specificity nor sensitivity of these found biomarkers in early diagnosis and therapy is satisfied. Therefore, identification of novel biomarker and effective treating target are urgently needed in terms of curing pancreatic cancer and prolonging the survival time of patients.

Armadillo repeat-containing X-linked protein (ARMCX) is a family of proteins which is encoded by genes with multiple armadillo repeats located on the X chromosome. Armadillo repeat-containing 10 (ARMC10), a close phylogenetically related gene, is considered to be the ancestor gene of ARMCX family [18]. This protein family localizes to the mitochondria, regulates mitochondrial dynamics and is well-known to regulate protein-protein interaction (PPI) involved in nuclear transport, cellular connection, and transcription activation [19,20]. Recent studies have shown that the members of the ARMCX family are involved in human carcinogenesis and tumor progression, such as lung, ovarian, gastric, colorectal and hepatocellular carcinomas, in terms of cell migration, cell proliferation, signal transduction and maintenance of integrating cell constitution [20–25]. However, the relationship and intrinsic mechanism between ARMC10 and PAAD is still indistinct.

Thus, to explore the role of ARMC10 in development and aggravation of PAAD, we viewed and analysed RNA sequencing data from TCGA, GEO datasets (http://www.tcga.org; https://www.ncbi.nlm.nih.gov/gds/) and a series of statistical and bioinformatics methods such as differentially expressed genes (DEGs) analysis, Kaplan-Meier (KM) survival analysis, logistic regression analysis, cox regression analysis, nomogram, gene ontology (GO) analysis, Kyoto Encyclopedia of Genes and Genomes (KEGG) pathway analysis, gene set enrichment analysis (GSEA) and single sample gene set enrichment analysis (ssGSEA). To deeply dig how ARMC10 acts in PAAD, we knockdown the expression of ARMC10 in vitro and gained more compelling evidence of how ARMC10 affects the ability of proliferation, invasion, and migration of PAAD cells.

2. Materials and methods

2.1. Data collection and preprocessing

The RNA expression level data and clinical characteristics of PAAD patients were acquired from TCGA (https://portal.gdc.cancer.gov/) and GEO (https://www.ncbi.nlm.nih.gov/gds/). The expression sets, GSE15471 and GSE16515 were used [26,27]. The exclusion criteria were overall-survival (OS) less than 30 days and normal pancreatic tissues. Transformed from the HTSeq-FPKM information of level 3, Transcripts Per Million (TPM) information of 179 pancreatic samples from TCGA were applied for following analyses. Unavailable clinical factors in 179 samples were viewed as missing values and the information were shown in Supplemental Table 1.

2.2. ARMC10 differentially expressed in PAAD tissues in the TCGA databases

We performed scatter plots and boxplots with considering disease state (normal and tumor) as variable to gauge unaccord expression of ARMC10. Receiver operating characteristic (ROC) curves were wielded to estimate the diagnostic capability of ARMC10. Expression of ARMC10 ranked below the median statistically was defined as ARMC10-low, and ARMC10-high as ARMC10 above the median.

2.3. The identification of DEGs between ARMC10-Low and -high expression PAAD groups

Applying student's t-test, DESeq2 (4.0) package was used to analyze DEGs between ARMC10-low and ARMC10-high samples from TCGA database. Differences with the absolute log2-fold change (FC) higher than 1.5 and the adjusted p value < 0.05 were considered to be statistically different. All of the DEGs were displayed in the volcano plots and heat map.

2.4. Functional enrichment and evaluation of immune related cell infiltration

To probe the enrichment of pertinent DEGs of ARMC10, Metascape (http://metasape.org) was applied by pathway and process. The criterion is set as following: the enrichment factor >1.5, a minimum count of 3, and P < 0.01 to attain saliently statistical differences. In order to analyze the ARMC10-related pathways and 6 phenotypes, we explored the discrimination on pathways between ARMC10-low and ARMC10-high patients and performed GSEA with the ARMC10 differentially expressed matrix. To scan the obvious changes in signal pathways, we performed a permutation test with 1000 times. FDR <0.25 and adjusted P < 0.01 were affirmed as significantly related genes. Using R package clusterProfiler (4.0), graphical plots and statistical analysis were performed. Applying STRING database, we selected the PPI pairs whose interaction score>0.95 by constructing the PPI network by DEGs. The ssGSEA was applied to query expression data of genes in published gene lists in order to quantify the relative infiltration levels of 24 types of immune cells, which included 509 genes, and the signatures applied contained a multiple set of innate and adaptive immune cell types. Spearman correlation and Wilcoxon test were used to demonstrate the association between the infiltration degree of immune cells and ARMC10, as well as the different groups of ARMC10 expression accompanied by immune cells infiltration.

2.5. Clinical evaluation on prognosis state, model construction and estimation

With the application of R package (V3.6.2), the compact correlation between ARMC10 and clinicopathological characteristics was analyzed integrally by logistic regression and Wilcoxon signed-rank sum test. For further exploration, we obtained and dig the clinical pathologic factors related to 10-year OS, disease-specific survival (DSS) and progression-free interval (PFI) from TCGA database using KM survival analysis and Cox regression. We chose Multivariate Cox analysis to construct the interior relationship between expression level of ARMC10 and series of clinical performance, such as survival rate and other clinical pathologic factors (T stage, M stage, pathologic stage, histologic grade, residual tumor, primary therapy outcome). Median of ARMC10 expression was set as the cut-off value. $P < 0.05$ was set as statistically significant in all tests we did above. Using KM analysis accompanied by a two-sided log rank test, we analyzed the difference of OS, DSS, PFI between ARMC10 -low and -high group. We used the independent prognostic factors acquired from multivariate Cox regression to construct a nomogram, so as to evaluate the survival potential for 1-, 3-, and 5-year, respectively. We constructed nomograms, which included calibration plots and significant clinical factors using RMS package (https://cran.r-project.org/web/packages/rms/index.html). Based on the observed occurrences, we drafted the nomogram predicted probabilities, and graphically evaluated the calibration curves, the 45° line indicated the best predictive values. 1000 resamples were calculated by a bootstrap approach, then we performed a concordance index (C-index), which was applied to estimate the discrimination power of this nomogram. Using C-index, we evaluated the separate prognostic factors and predictive accuracies of the nomogram. All the statistical tests in this research were two tailed and the statistical significance level was set at 0.05.

2.6. Cell culture and transfection

PAAD cell lines (HPNE, AsPC-1, BxPC-3, CFPAC-1, Mia, Panc-1, PATU8988) were acquired from the American Type Culture Collection (Virginia, USA). The cells were cultured in Dulbecco's Modified Eagle Medium (Hyclone) with 10% fetal bovine serum (Gibco) and incubated at 37 °C with 5% carbon dioxide. The siARMC10-1 (5′-GGAGAUUCUUCUUCGAGUATT-3′), siARMC10-2 (5′-GGAUGGAUGUAUAAUUAAAUU-3′) and si-Control were bought from RiboBio (Guangzhou, China) and introduced into cells at a concentration of 50 nM. Transfections were performed using OPTI-MEM (Invitrogen) and Lipofectamine 3000 under the manufacturer's instructions. After that, the cells were harvested for 48 h.

2.7. Western blotting

The cells were cultured till the confluence reached 70%. The western blotting (WB) was performed as previously recorded. In brief, 25 μg proteins were subjected to Sodium Dodecyl Sulfate-Polyacrylamide Gel Electrophoresis (SDS-PAGE) using a 10% gel. The WB experiment was performed using the anti-ARMC10 at 1:1000 dilution (Catalog number: 20506-1-AP) and anti-GAPDH at 1:5000 dilution (Catalog number: 10494-1-AP) bought from Proteintech Group (Rosemont, United States).

2.8. Immunofluorescence

The immunofluorescence assays were performed using anti-ARMC10 (Abcam, 1:300) according to the manufacturer's protocol. The primary antibody used in this study was against ARMC10 (20506-1-A). The cells were incubated with the corresponding ARMC10-conjugated secondary antibodies (Abcam, 1:200). 0.1% DAPI was used to stain the nucleus for 30 min 2 h later. Images were detected using confocal microscopy (Leica, Jena, Germany).

2.9. Cell proliferation, invasion, and migration assays

To detect the proliferation level of PAAD cells in different groups, we used the Cell Counting Kit-8 (CCK-8) and colony formation assays. A total of 2500 PAAD cells were added into each well of 96-well plate with 10 μL of CCK-8 solution (Beijing Solarbio Science & Technology Co., Ltd, Bei, China). After an incubation at 37 °C for 2 h, the absorbance of each well was analyzed at 450 nm. In colony formation experiment, 1000 cells in different groups were added into each well of 6-well plate. The cell culture medium was replaced every 72 h. When the appearance of colonies showing, crystal violet and 4% paraformaldehyde were applied to stain and fix the cells. As previous research, the wound healing and transwell assays were used to evaluate the ability of cellular invasion and migration [28].

2.10. Statistical analysis

RStudio software and the R software (version 3.8.0) were used for statistical analyses. Data analyses were processed using one-way analysis of variance (ANOVA) and two-tailed Student's t-test. Statistically significance of the difference was set at p–value <0.05.

3. Results

3.1. ARMC10 expression in pan-cancers and PAAD

We analyzed the expression data of pan-cancer tissues and normal controls based on TCGA and Genotype-Tissue Expression (GTEx) datasets. ARMC10 expression was significantly elevated in adrenocortical carcinoma (ACC), bladder urothelial carcinoma (BLCA),

breast filtrating carcinoma (BRCA), cholangiocarcinoma (CHOL), colon adenocarcinoma (COAD), diffuse large B cell lymphoma (DLBCL), esophageal carcinoma (ESCA), pleomorphic glioma (GBM), Head and Neck squamous cell carcinoma (HNSC), renal clear cell carcinoma (KIRC), renal papillary cell carcinoma (KIRP), brain low grade glioma (LGG), liver hepatocellular carcinoma (LIHC), lung adenocarcinoma (LUAD), lung squamous cell carcinoma (LUSC), ovarian serous cystadenocarcinoma (OV), PAAD, prostate cancer (PRAD), rectum adenocarcinoma (READ), skin melanoma (SKCM), gastric cancer (STAD), testicular germ cell tumors (TGCT), thyroid cancer (THCA), thymic cancer (THYM), endometrial cancer (UCEC) and down-regulated in acute myeloid leukemia (LAML) based on the Wilcoxon test ($P < 0.05$; Fig. 1A). Besides, to detect the diagnostic effects of ARMC10, which was found to be higher expressed in tumor tissues than that in normal controls in three different datasets ($P < 0.05$; Fig. 1B–D), the ROC curves were plotted. As shown in Fig. 1E, the area under the curve (AUC) of ARMC10 is 0.957, indicating it may be a potential diagnostic biomarker for PAAD.

3.2. Recognition of DEGs in PAAD with high/low ARMC10 expression

We compared 90 ARMC10-high PAAD samples with 89 ARMC10-low PAAD samples and found a total of 668 DEGs with statistical significance (adjusted p-value <0.05, absolute log2-FC> 1.5) (Fig. 1F; Supplementary Table 2). Using DESeq2 package, we analyzed DEGs in HTSeq-Counts. The top 10 DEGs ranked by relative expression were shown in Fig. 1G.
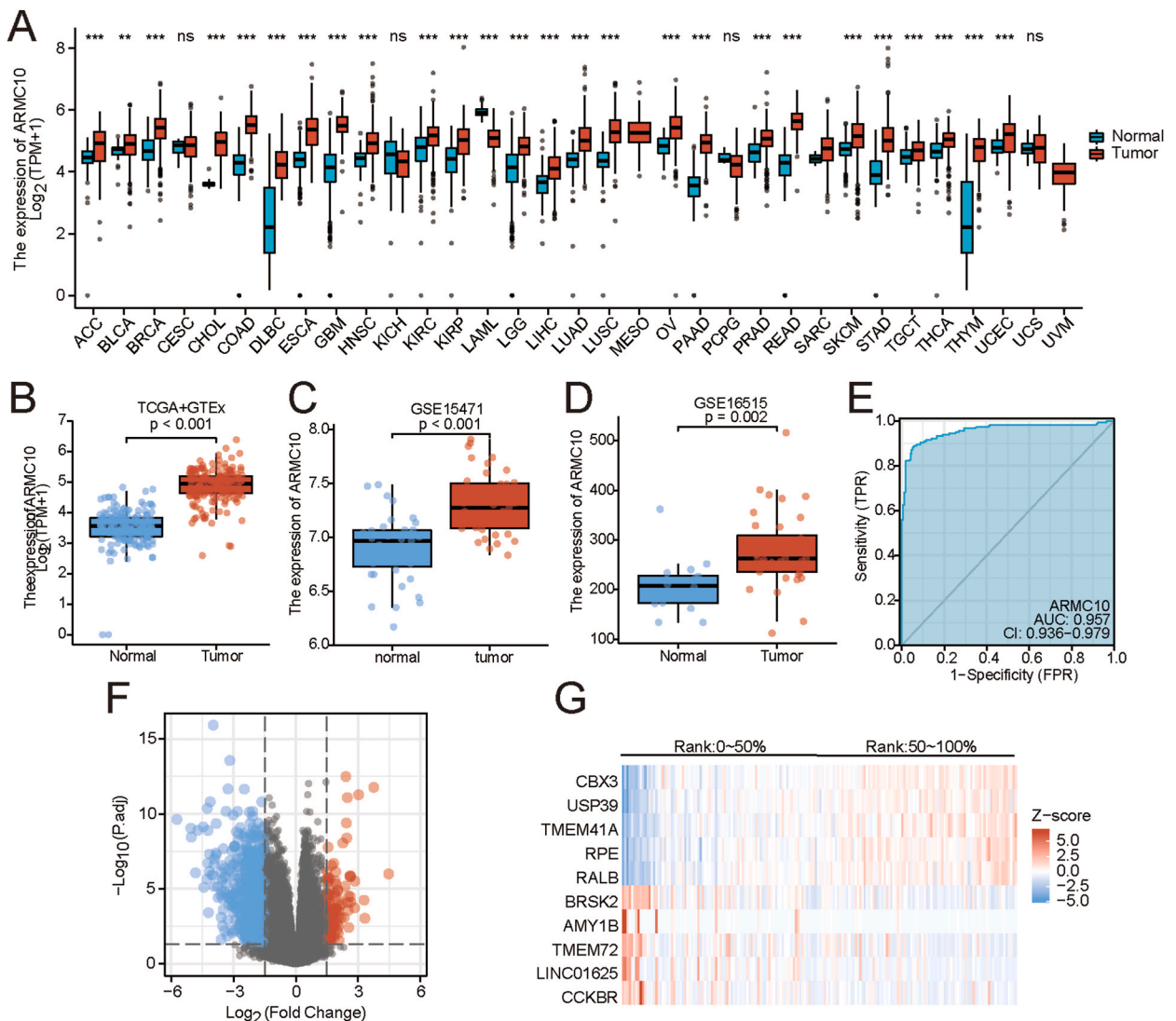

Fig. 1. | The expression levels of ARMC10 in pan-cancer tissues and ARMC10-related differentially expressed genes (DEGs). (A) Increased or decreased ARMC10 expression in different cancers compared with normal tissues in the TCGA and GTEx database. (B–D) The expression levels of ARMC10 in PAAD compared with normal in the TCGA and GEO datasets. (E) A ROC curve to test the diagnostic effect of ARMC10 in pancreatic cancer tissues was drawn. (F) Volcano plot of the DEGs. (G) The top 10 DEGs ranked by relative expression.

3.3. Functional enrichment analysis of ARMC10-associated genes in PAAD

To further study the biological functions of ARMC10-associated genes, the DEGs were subjected to the GO analysis using Metascape and classified into Biological Processes (BPs), Cellular Components (CCs), and Molecular Functions (MFs) categories. The results showed that cellular potassium ion transport, regulation of membrane potential, glutamate receptor signaling pathway, cation channel complex, transmembrane transporter complex, glutamate receptor activity and growth factor activity were significantly enriched (Fig. 2A; Supplementary Table 3). It indicated that these pathways might relate to modulation of ARMC10-associated genes.

3.4. Protein-protein interaction (PPI) network analysis

A PPI network was framed grounded on the STRING dataset to identify the association among the 1033 DEGs in PAAD group with the high confidence of interaction score was set as 0.70. We found that 311 proteins and 566 edges presented significant disease associations and 16 clusters of hub genes were picked from the PPI network with scores ≥5000 (Supplementary Fig. 1A-Q; Supplementary Table 4). Thereinto, the top 10 hub genes were CBX3, USP39, TMEM41A, RPE, RALB, BRSK2, AMY1B, TMEM72, LINC01625 and CCKBR.
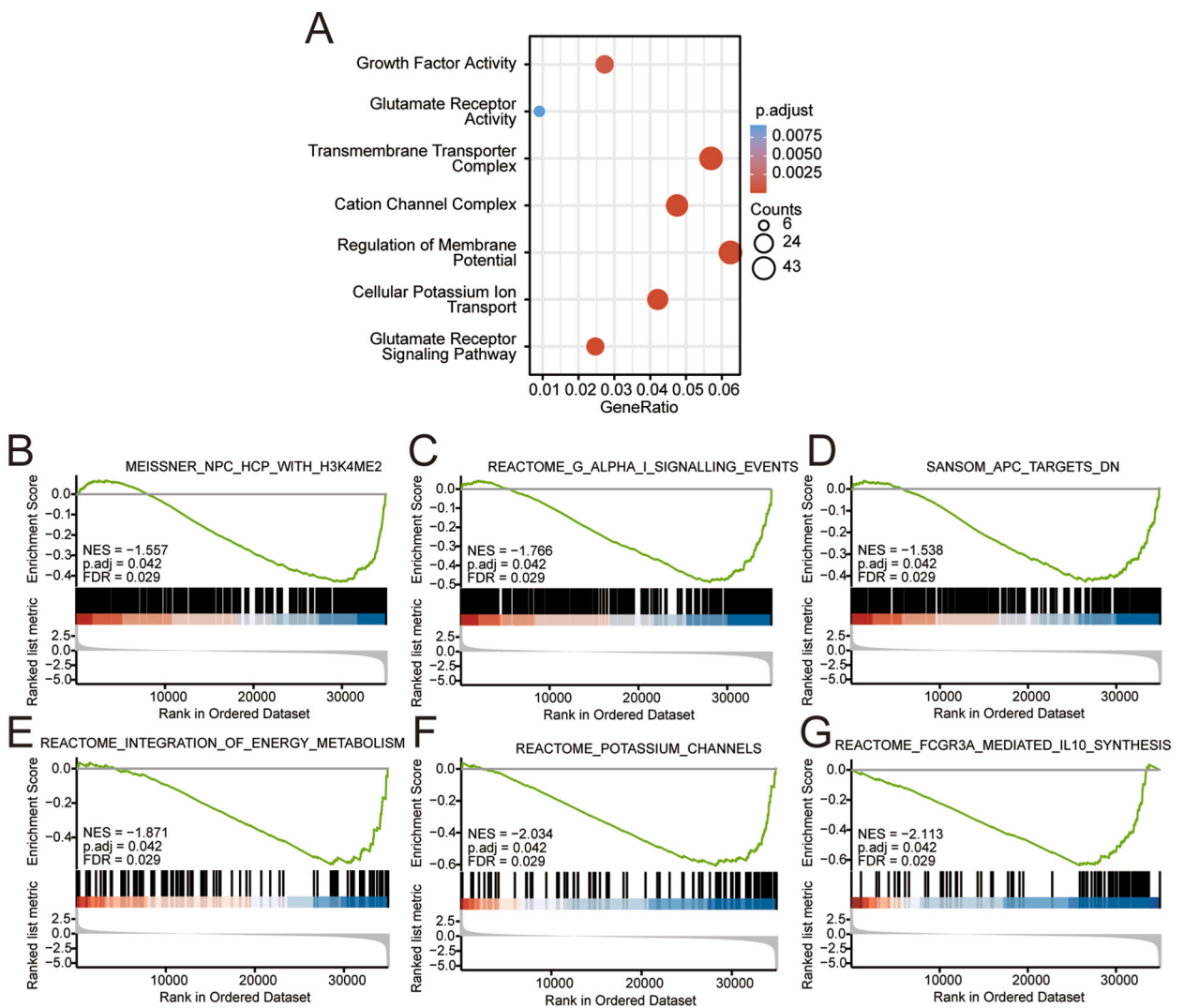

Fig. 2. | GO annotations of ARMC10-associated genes significantly enriched in PAAD. (A) Top 7 of biological process enrichment relevant to ARMC10-associated genes with plot graph. (B–G) Enrichment plots from the gene set enrichment analysis (GSEA). Several pathways and biological functions were differentially enriched in ARMC10-associated PAAD, including Genes with high-CpG-density promoters (HCP) bearing histone H3 dimethylation mark at K4 (H3K4me2) in neural precursor cells (NPC), G alpha (i) signaling events, APC targets, integration of energy metabolism, potassium channels, FCGR3A mediated IL10 synthesis. NES, normalized enrichment score; p.adj, adjusted P value; FDR, false discovery rate.
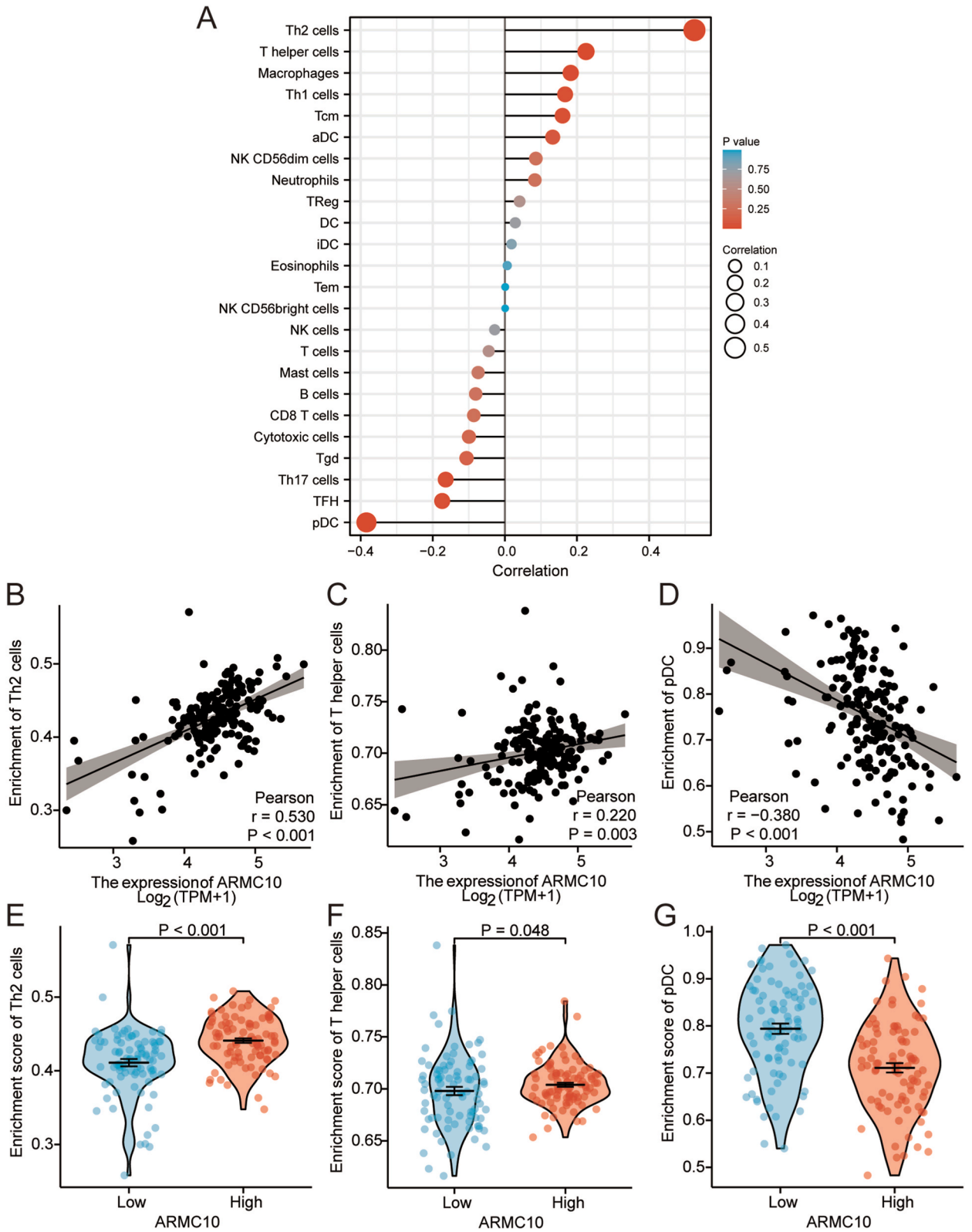
(caption on next page)

Fig. 3. | Relevance Between ARMC10 Expression Level and Immune Infiltration. (A) Correlation between the ARMC10 expression level and relative abundances of 24 types of immune cells. The size of dots indicates the absolute value of Spearman R. (B–G) Correlation diagrams and scatter plots showing the differentiation of T helper 2 (Th2) cells, T helper cells, and plasmacytoid dendritic cells (pDC) infiltration level between ARMC10 high and low groups.

3.5. Potential mechanism of ARMC10 in the progression of PAAD

Using GSEA, we compared the expression data between ARMC10-high and -low samples to excavate ARMC10-related signaling pathways and significant differences (nominal, NOM p value < 0.05; false discovery rate, FDR q value < 0.25) in enrichment of the Molecular Signatures Database (MSigDB) Collection (c2.cp.reactome/biocarta/kegg.v6.2.symbols.gmt). The top significantly enriched pathways were selected according to their normalized enrichment score (NES). Enrichment plots of GSEA showed that Genes with high-CpG-density promoters (HCP) bearing histone H3 dimethylation mark at K4 (H3K4me2) in neural precursor cells (NPC), G alpha (i) signaling events, APC targets, integration of energy metabolism, potassium channels, FCGR3A mediated IL10 synthesis, were significantly enriched in ARMC10-high patients (Fig. 2B–G; Supplementary Table 5).

3.6. Relevance between ARMC10 expression level and immune infiltration

In previous studies, higher ARMC10 was shown to be related to shorter survival and poorer response to immunotherapy in glioblastoma and melanoma [29,30]. And immune cell infiltration was a significant indicator of immune microenvironment of pancreatic cancer and was associated with immunotherapy response and survival in PAAD patients [31,32]. So, we hypothesized that ARMC10

Table 1

| Relevance between ARMC10 expression level and clinicopathological variables.

Characteristic	levels	Low expression of ARMC10	High expression of ARMC10	p
n		89	89	
T stage, n (%)	T1	4 (2.3%)	3 (1.7%)	0.024
	T2	18 (10.2%)	6 (3.4%)	
	T3	63 (35.8%)	79 (44.9%)	
	T4	2 (1.1%)	1 (0.6%)	
N stage, n (%)	N0	26 (15%)	24 (13.9%)	0.829
	N1	60 (34.7%)	63 (36.4%)	
M stage, n (%)	M0	35 (41.7%)	44 (52.4%)	0.386
	M1	1 (1.2%)	4 (4.8%)	
Pathologic stage, n (%)	Stage I	15 (8.6%)	6 (3.4%)	0.069
	Stage II	68 (38.9%)	78 (44.6%)	
	Stage III	2 (1.1%)	1 (0.6%)	
	Stage IV	1 (0.6%)	4 (2.3%)	
Radiation therapy, n (%)	No	55 (33.7%)	63 (38.7%)	0.398
	Yes	25 (15.3%)	20 (12.3%)	
Primary therapy outcome, n (%)	PD	19 (13.7%)	30 (21.6%)	0.261
	SD	3 (2.2%)	6 (4.3%)	
	PR	4 (2.9%)	6 (4.3%)	
	CR	39 (28.1%)	32 (23%)	
Age, n (%)	≤65	48 (27%)	45 (25.3%)	0.764
	>65	41 (23%)	44 (24.7%)	
Race, n (%)	Asian	5 (2.9%)	6 (3.4%)	0.285
	Black or African American	1 (0.6%)	5 (2.9%)	
	White	81 (46.6%)	76 (43.7%)	
Gender, n (%)	Female	43 (24.2%)	37 (20.8%)	0.451
	Male	46 (25.8%)	52 (29.2%)	
Histologic grade, n (%)	G1	24 (13.6%)	7 (4%)	0.001
	G2	44 (25%)	51 (29%)	
	G3	18 (10.2%)	30 (17%)	
	G4	2 (1.1%)	0 (0%)	
Residual tumor, n (%)	R0	61 (37.2%)	46 (28%)	0.020
	R1	18 (11%)	34 (20.7%)	
	R2	3 (1.8%)	2 (1.2%)	
Anatomic neoplasm subdivision, n (%)	Head of Pancreas	70 (39.3%)	68 (38.2%)	0.857
	Other	19 (10.7%)	21 (11.8%)	
Alcohol history, n (%)	No	34 (20.5%)	31 (18.7%)	0.658
	Yes	48 (28.9%)	53 (31.9%)	
Smoker, n (%)	No	36 (25%)	29 (20.1%)	0.482
	Yes	38 (26.4%)	41 (28.5%)	
History of chronic pancreatitis, n (%)	No	68 (48.2%)	60 (42.6%)	0.076
	Yes	3 (2.1%)	10 (7.1%)	
History of diabetes, n (%)	No	52 (35.6%)	56 (38.4%)	0.774
	Yes	20 (13.7%)	18 (12.3%)	

might correlate with immune cell infiltration in PAAD.

The ssGSEA was performed in PAAD samples and relevance between ARMC10 expression level and immune infiltration was demonstrated using Spearman correlation. As shown in Fig. 3, the expression level of ARMC10 was positively relevant to the abundance of T helper 2 (Th2) cells (R = 0.530, P < 0.001), T helper cells (R = 0.220, P = 0.003) and negatively related to the abundance of plasmacytoid dendritic cells (pDC) (R = −0.380, P < 0.001).
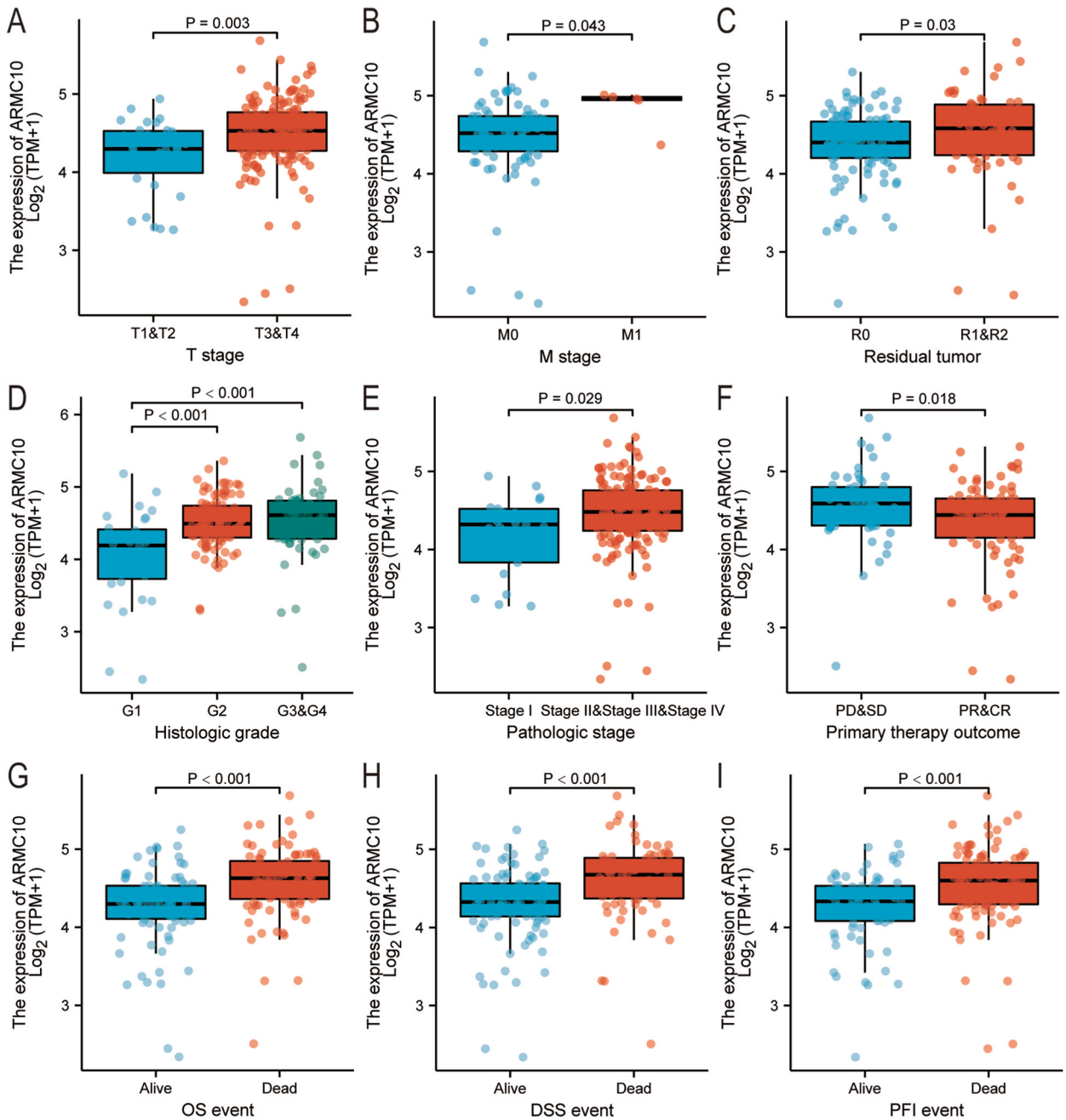

Fig. 4. | Relevance between ARMC10 expression level and clinicopathological variables, including (A) T stage, (B) M stage, (C) Residual tumor, (D) Histologic grade, (E) Pathologic stage, (F) Primary therapy outcome, (G) OS event, (H) DSS event, and (I) PFI event in PAAD patients in TCGA cohort. OS, Overall survival; DSS, Disease-specific survival; PFI, Progression-free interval; TCGA, The Cancer Genome Atlas; PAAD, Pancreatic adenocarcinoma.

3.7. Relevance between ARMC10 expression level and clinicopathological variables

To better seize the clinical relevance of ARMC10 expression in PAAD, we explored its association with clinical characteristics of PAAD patients from TCGA. As the results showed, higher ARMC10 expression was relevant to clinical T stage (T3&4 vs. T1&2, P = 0.003), clinical M stage (M1 vs. M0, P = 0.043), pathologic stage (Stage II-IV vs. Stage I, P = 0.029), residual tumor (R1&2 vs. R0, p = 0.03), histologic grade (G3/G4 vs. G1, P < 0.001; G2 vs. G1, P < 0.001), primary therapy endpoint (PR&CR vs. PD&SD, P = 0.018), OS event (Dead vs. Alive, P < 0.001), DSS event (Dead vs. Alive, P < 0.001) and PFI event (Dead vs. Alive, P < 0.001) (Table 1, Fig. 4). Using univariate logistic regression, we found that ARMC10 expression level in PAAD was positively associated with T stage (T3&4 vs. T1&2, OR = 5.122, P = 0.003), pathologic stage (Stage II-IV vs. Stage I, OR = 4.609, P = 0.011), primary therapy outcome (PR&CR vs. PD&SD, OR = 0.353, P = 0.040), Residual tumor (R1&2 vs. R0, OR = 2.757, P = 0.034) (Table 2). The results above indicated that PAAD patients with higher ARMC10 expression were more likely to develop into advanced stage.

3.8. Relevance between ARMC10 expression level and prognosis of PAAD patients

As shown in Fig. 5A-C, patients with higher expression of ARMC10 have lower OS (HR = 2.45, P < 0.001), DSS (HR = 2.57, P < 0.001), and PFI (HR = 2.12, P < 0.001) compared to those with lower expression. Furthermore, we performed subgroup analysis and found that higher ARMC10 expression had prognostic value for lower OS in PAAD patients of T1-T4 stage, N0& N1, pathologic stage I& II, G1& G2 histologic grade, head of pancreas neoplasm and male (Fig. 5D–K). We also performed subgroup analysis of DSS and PFI in PAAD patients with high ARMC10 expression (Seen in Supplementary Tables 8 and 9). Besides, we did univariate Cox regression and discovered that higher ARMC10 expression was correlated to lower OS (HR: 2.424; CI: 1.567–3.750; P < 0.001; Table 3), DSS (HR: 2.560; CI: 1.555–4.216; P < 0.001; Supplementary Table 6) and PFI (HR: 2.246; CI: 1.506–3.349; P < 0.001; Supplementary Table 7). Then using multivariate Cox regression, we excavated factors correlated to prognosis including ARMC10 expression, anatomic neoplasm subdivision, histology grade, residual tumor, T, N and pathologic stage, radiation therapy and primary therapy outcome. It showed that high ARMC10 was also relevant to poor OS (HR: 2.797; CI: 1.581–4.950; P < 0.001; Table 3), DSS (HR: 2.681; CI: 1.432–5.018; P = 0.002; Supplementary Table 6) and PFI (HR: 2.063; CI: 1.227–3.468; P = 0.006; Supplementary Table 7). Selected from Cox regression results, multiple subgroups of PAAD patients with higher ARMC10 expression had lower OS, DSS and PFI (Seen in Table 4, Supplementary Tables 8 and 9).

3.9. A nomogram constructed to predict survival rates of PAAD patients

We further constructed a nomogram based on ARMC10 expression and some related clinicopathologic variables to predict the survival rates of PAAD patients (Fig. 6A). The point scale of nomogram was set as 0–100 assigned to the variables according to the multivariate Cox regression and the total scores were calculated. The predictive value of each variable for prognosis was defined as vertical dimension from the total score axis to the outcome axis. For instance, a PAAD patient with high ARMC10 expression (97.5 points), N1 stage (62 points), R0 residual (0 points), G3 histologic grade (55 points) tumor located on head of pancreas (80 points), radiation therapy YES (0 points), PD (77.5 points) has a total point of 372. Correspondingly, the 1-, 3- and 5-year survival probability are 65%, 14% and 6%, respectively. Then using Hosmer test of the calibration curve, we evaluated the predictive validity of the nomogram in the TCGA-PAAD cohort. The C-index was 0.727 (95% CI 0.696–0.758), indicating a moderate predictive accuracy of this nomogram model (Fig. 6B).

Table 2

| Univariate logistic regression between ARMC10 expression level and clinical characteristics.

| Characteristics	Total(N)	Odds Ratio (OR)	P value
T stage (T3&T4 vs. T1&T2)	176	5.122 (1.804–15.704)	0.003
N stage (N1 vs. N0)	173	1.208 (0.480–3.010)	0.685
M stage (M1 vs. M0)	84	15.330 (0.839–469.031)	0.080
Pathologic stage (Stage II&Stage III&Stage IV vs. Stage I)	175	4.609 (1.432–15.426)	0.011
Radiation therapy (Yes vs. No)	163	0.928 (0.378–2.330)	0.872
Primary therapy outcome (PR&CR vs. PD&SD)	139	0.353 (0.124–0.913)	0.040
Gender (Male vs. Female)	178	1.520 (0.684–3.459)	0.307
Race (White vs. Asian&Black or African American)	174	0.422 (0.096–1.673)	0.236
Age (>65 vs. ≤ 65)	178	1.047 (0.472–2.335)	0.910
Residual tumor (R1&R2 vs. R0)	164	2.757 (1.120–7.370)	0.034
Histologic grade (G3&G4 vs. G1&G2)	176	1.788 (0.730–4.636)	0.215
Anatomic neoplasm subdivision (Other vs. Head of Pancreas)	178	0.836 (0.328–2.180)	0.708
Smoker (Yes vs. No)	144	1.249 (0.524–3.020)	0.615
Alcohol history (Yes vs. No)	166	1.124 (0.481–2.620)	0.784
History of diabetes (Yes vs. No)	146	0.564 (0.211–1.493)	0.246
History of chronic pancreatitis (Yes vs. No)	141	3.447 (0.708–19.167)	0.141
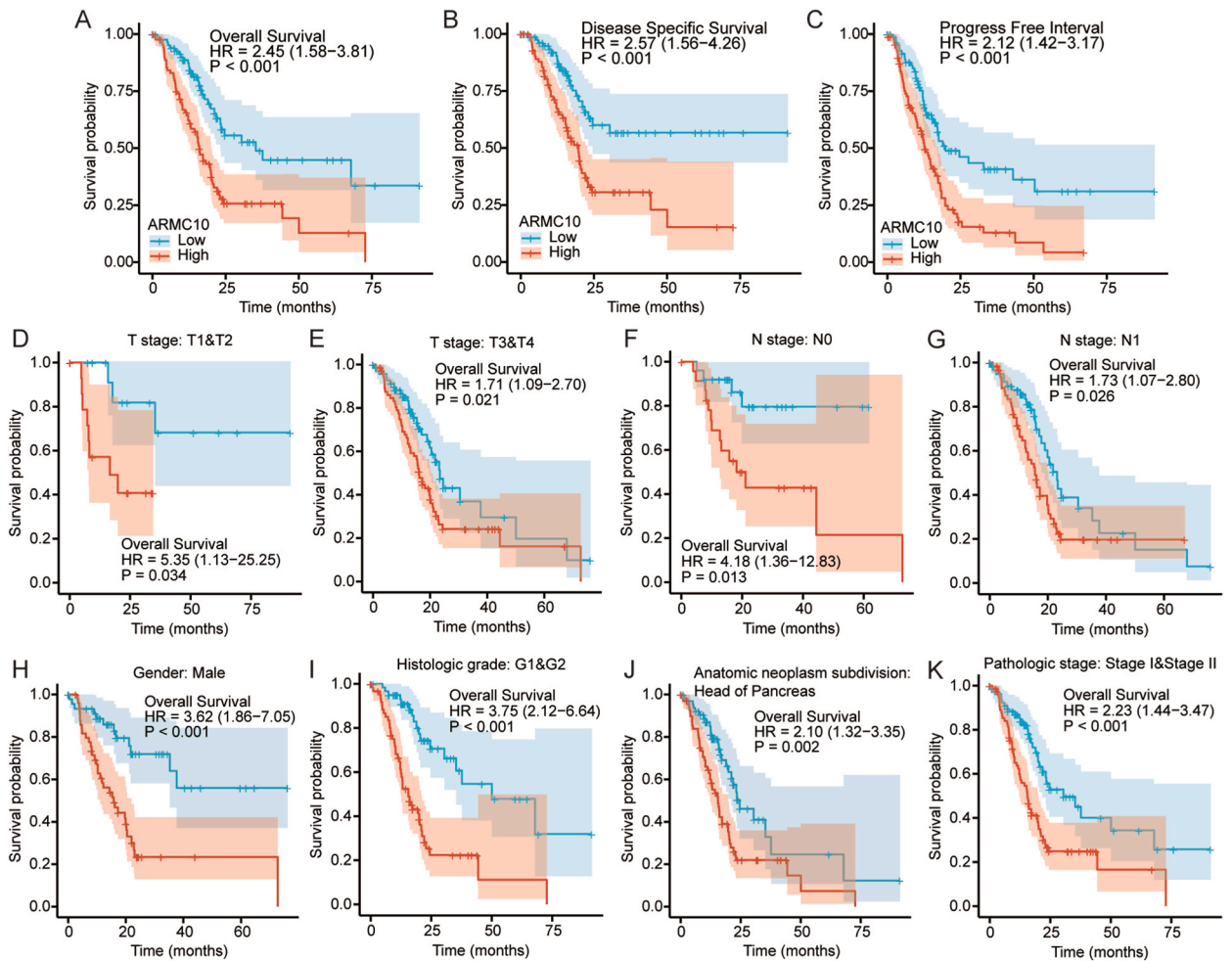
Fig. 5. | Kaplan Meier survival curve indicating relevance between ARMC10 expression level and prognosis of PAAD patients. (A–C) Survival curves of OS, DSS, and PFI between ARMC10 -high and -low PAAD patients. (D–K) OS survival curves of T stage 1&2, T stage 3&4, N stage: N0&1, pathologic stage I&II, gender: male, histologic grade: G1&G2, head of pancreas subgroups between ARMC10-high and -low PAAD patients. PAAD, Pancreatic adenocarcinoma; OS, Overall survival; DSS, Disease-specific survival; PFI, Progression-free interval.

Table 3

| Univariate and multivariate survival results (Overall Survival) of prognostic covariates in PAAD patients.

Characteristics	Total(N)	Univariate analysis		Multivariate analysis	
		Hazard ratio (95% CI)	P value	Hazard ratio (95% CI)	P value
T stage (T3&T4 vs. T1&T2)	176	2.023 (1.072–3.816)	**0.030**	1.099 (0.385–3.139)	0.860
N stage (N1 vs. N0)	173	2.154 (1.282–3.618)	**0.004**	2.355 (1.086–5.107)	**0.030**
M stage (M1 vs. M0)	84	0.756 (0.181–3.157)	0.701		
Pathologic stage (Stage II&Stage III&Stage IV vs. Stage I)	175	2.291 (1.051–4.997)	**0.037**	0.391 (0.084–1.824)	0.232
Radiation therapy (Yes vs. No)	163	0.508 (0.298–0.866)	**0.013**	0.381 (0.196–0.742)	**0.005**
Primary therapy outcome (CR&PR vs. PD&SD)	139	0.425 (0.267–0.677)	**<0.001**	0.489 (0.289–0.826)	**0.007**
Gender (Male vs. Female)	178	0.809 (0.537–1.219)	0.311		
Race (White vs. Asian&Black or African American)	174	1.161 (0.582–2.318)	0.672		
Age (>65 vs. ≤ 65)	178	1.290 (0.854–1.948)	0.227		
Residual tumor (R1&R2 vs. R0)	164	1.645 (1.056–2.561)	**0.028**	1.438 (0.841–2.458)	0.184
Histologic grade (G3&G4 vs. G1&G2)	176	1.538 (0.996–2.376)	0.052	1.709 (0.974–2.997)	0.062
Anatomic neoplasm subdivision (Other vs. Head of Pancreas)	178	0.417 (0.231–0.754)	**0.004**	0.418 (0.194–0.900)	**0.026**
ARMC10 (High vs. Low)	178	2.424 (1.567–3.750)	**<0.001**	2.797 (1.581–4.950)	**<0.001**

Table 4

| The prognostic value of ARMC10 (Overall Survival) in multiple PAAD subgroups.

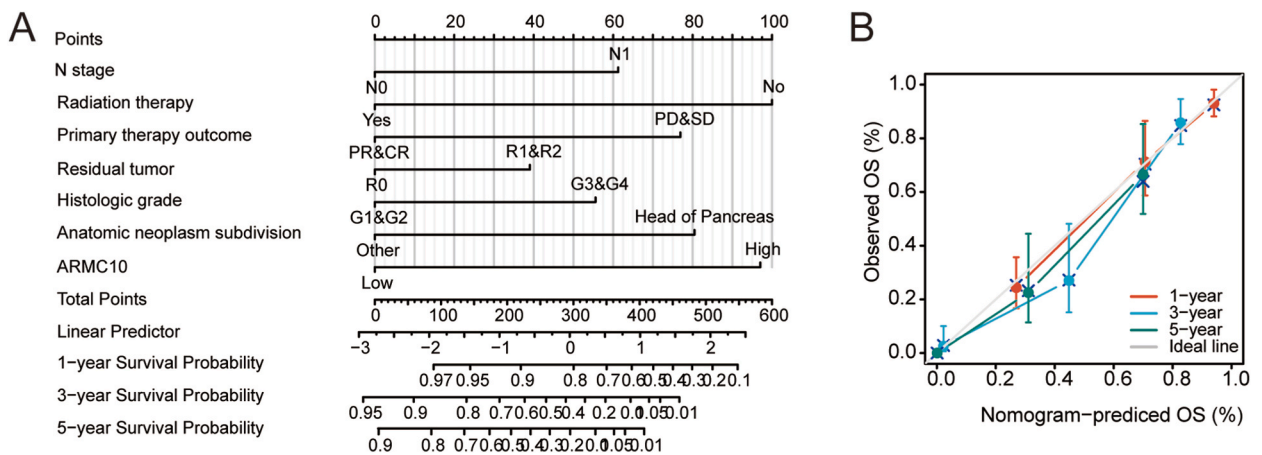| Characteristics	N (%)	HR (95% CI)	P value
T stage			
T1&T2	31 (17.6%)	5.35 (1.13–25.25)	0.034
T3&T4	145 (82.4%)	1.71 (1.09–2.70)	0.021
N stage			
N0	50 (28.9%)	4.18 (1.36–12.83)	0.013
N1	123 (71.1%)	1.73 (1.07–2.80)	0.026
M stage			
M0	79 (94%)	1.64 (0.85–3.16)	0.140
M1	5 (6%)	–	–
Pathologic stage			
Stage I-Stage II	167 (95.4%)	2.23 (1.44–3.47)	0.000
Stage III-Stage IV	8 (4.6%)	–	–
Histologic grade			
G1& G2	126 (71.6%)	3.75 (2.12–6.64)	0.000
G4&G3	131 (37)	1.05 (0.52–2.13)	0.886

Fig. 6. | A predictive method of PAAD patients' 1-, 3- and 5-year survival probability. (A) A nomogram constructed to predict the 1-, 3- and 5-year survival probability of PAAD patients. (B) Calibration curve of the nomogram for estimating the probability of OS at 1, 3, and 5 years. C-index 0.727 (95% CI 0.696–0.758). PAAD, Pancreatic adenocarcinoma; OS, overall survival.

3.10. Knockdown of ARMC10 alleviated malignant phenotype of PAAD in vitro

To better recognize the role of ARMC10 in PAAD, we observed the expression of ARMC10 in some PAAD cell lines (HPNE, CFPAC-1, Aspc-1, Bxpc-3, Panc-1, PATU8988, Mia). As shown in Fig. 7A, the expression level of ARMC10 was higher in Bxpc-3 and Aspc1 than in other cell lines. Thus, further analysis was performed in Bxpc-3 and Aspc1 cell lines. Using western blotting, the transfection efficiency of si-ARMC10-1 and si-ARMC10-2 were identified (Fig. 7B, Supplementary Fig. 3). The immunofluorescence assay showed that ARMC10 expression was significantly decreased after knockdown ARMC10 (Fig. 7C). We performed colony formation and CCK8 experiments and the results showed that inhibition of ARMC10 could lead to lower proliferation and colony formation rate in Bxpc-3 and Aspc1 cells (Fig. 7D–F). Besides, the result of wound healing assay showed that lower expression of ARMC10 could restrain the migration ability of Bxpc-3 and Aspc1 cells (Fig. 7G and H and Supplementary Figs. 2A and B). Then using transwell experiment, we found that cells after ARMC10 knockdown had lower invasion ability (Fig. 7I and J). These results demonstrated that ARMC10 played an important role in PAAD progression. Further studies are required to excavate the underlying mechanisms.

4. Discussion

The armadillo genes, also named as X-linked (ARMCX or ALEX) for being clustered on the X chromosome, encode a new family of proteins [18]. They are reported to be connected with many biological processes, such as embryogenesis and tumorigenesis, cell assembly, RNA modification, DNA replication, nuclear transport, mitochondrial fission and fusion, transport in neurons and execute different functions through binding its armadillo repeat domain with different binding partners [19,20,33,34]. Research demonstrated that ARMCX proteins regulate mitochondrial dynamics and trafficking in neurons through interacting with the Kinesin/Miro/Trak2 complex [19]. ARMC10 alteration in neurons regulate mitochondrial trafficking through KIF5/Miro1-2/Trak2 complex [18]. Besides, phosphorylation of the S45 site of ARMC10 participating in regulating mitochondrial fission and fusion through AMPK-dependent
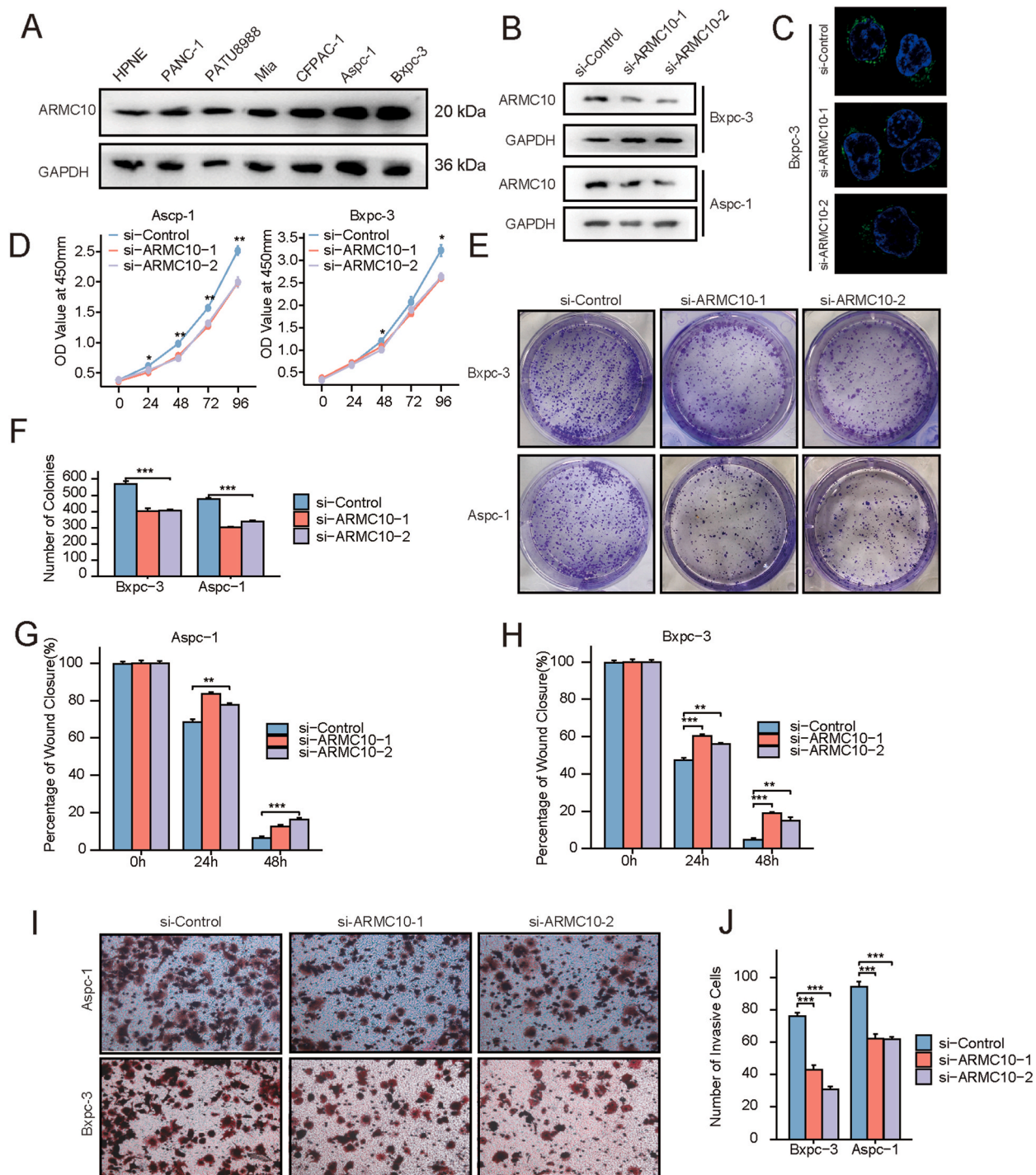
Fig. 7. | Knockdown of ARMC10 inhibits proliferation, migration, invasion ability and colony formation rate of PAAD cells in vitro. (A) The expression of ARMC10 in the HPNE, CFPAC-1, Aspc-1, Bxpc-3, Panc-1, PATU8988 and Mia cell lines were observed by western blotting, respectively. (B) The transfection efficiency of si-ARMC10 in the Bxpc-3 and Aspc1 cell lines detected by western blotting. (C) The effect of si-ARMC10 on the expression of ARMC10 in the Bxpc-3 cell line assessed by immunofluorescence. (D) The efficiency of si-ARMC10 on the proliferation of Bxpc-3 and Aspc1 cell lines using CCK8 assay. (E) Colony formation images after knockdown of ARMC10 in the Bxpc-3 and Aspc1 cell lines. (F) Concretized statistical analysis of the colony formation assay, including control, si-control, and si-ARMC10 groups in the Bxpc-3 and Aspc1 cell lines. (G, H) Concretized images and statistical analysis of the wound healing assay after knockdown of ARMC10 in the Bxpc-3 and Aspc1 cell lines. (I) Transwell assay images after knockdown of ARMC10 in the Bxpc-3 and Aspc1 cell lines. (J) Concretized statistical analysis of the transwell assay. *$p < 0.05$, **$p < 0.01$, and ***$p < 0.001$.

signaling pathways [35]. Several previous studies have demonstrated that ARMCX are related to the process of several diseases, especially in several carcinomas. ALEX1 and ALEX2 was speculated to be novel tumor suppressors in several human carcinomas, such as lung, prostate, colon, pancreas and ovarian [23]. The lost or significantly reduced expression of ALEX1 in colorectal and pancreatic cell lines were found to be regulated by cAMP-response element binding protein (CREB) and Wnt/β-catenin signaling in transcriptional level [36]. Besides, ARMCX also was verified to be a potential prognostic indicator of gastric carcinoma. The combination of lower ARMCX1 and ARMCX2 was related to higher OS [20]. ARMCX, located at the outer membrane of mitochondria, was reported to promote signal transduction between mitochondria and nucleus through interactions with Sox10 [37]. Down-regulation of ARMCX3 also was reported to have a protective effect against hepatocarcinogenesis mediated through Sox9 by affecting hepatic cell proliferation [25]. Through AKT/Slug/E-cadherin pathway, ALEX3 could inhibit the invasion of non-small cell lung cancer and predict clinical outcome [21]. Previous research has identified an ARMC10-BRAF fusion in malignant melanoma [38]. But research about ARMC10 in carcinomas are still facing a severe shortage.

In our study, we discovered that ARMC10 was differentially expressed in several types of cancers, including PAAD. The prognostic effect of ARMC10 in PAAD is relatively high with an AUC of 0.957. We then performed GO and GSEA to excavate the function of ARMC10. We discovered that ARMC10 was significantly relevant to glutamate receptor activity and signaling pathway, cellular potassium ion transport, cation channel complex, transmembrane transporter complex. Several studies have illustrated the role of glutamate receptor in the pathophysiology mechanisms underlying multiple cancers [39–44]. Glutamate receptor GRIA3 could reduce apoptosis and enhanced tumor cell proliferation and migration [45]. Metabotropic glutamate receptor 1 (mGluR1) is overexpressed in multiple tumor cells and is a promising drug target [46]. mGluR1 was regulated by the long non-coding RNA (lncRNA) HOXA distal transcript antisense RNA (HOTTIP) in pancreatic cancer. Altered levels of HOTTIP and mGluR1 were related to tumor cell viability, survival, migration, invasion, and apoptosis and acted as a potential prognostic marker [47]. Besides, researches have demonstrated the critical role of cation channels in the progression of various type of cancer, especially transient receptor potential cation channel subfamily V member 4 (TRPV4) [48–50], transient receptor potential cation channel subfamily M member 7/8 (TRPM7/8) [51–54] and two-pore channel 2 (TPC2) [55,56]. TPC2 is one of the cation channels located on endolysosomal membranes that could speed up movement between organelles and regulate phagocytosis, autophagy and lysosomal exocytosis [55]. In HCC, TPC2 knockout inhibited cell proliferation and tumor growth through affecting energy metabolism [56]. Another nonselective cation channel TRPM7 involved in Ca^{2+} and Mg^{2+} homeostasis maintenance has been found to manage cell differentiation, proliferation and migration. TRPM7 suppression in triple-negative breast cancer (TNBC) cells could amplify tumor necrosis factor-related apoptosis-inducing ligand (TRAIL)- induced antiproliferation and apoptosis [54]. In PAAD, TRPM7 was higher expressed in tumor tissues compared to the normal and correlated to poor prognosis. The study unveiled that TRPM7 affected BxPC-3 cell migration via a Mg^{2+}-dependent mechanism [53]. But the precise mechanism in PAAD is still unclear. From the GSEA results, we similarly found potassium channels were enriched. Potassium channel modulatory factor 1 (KCMF1) has previously been found to be upregulated in PAAD tissues with a pro-oncogenic function affecting tumor progression [57]. The potassium channel K_V 11.1 in PDAC cells exerts a critical role on cell migration and metastatic progression through f-actin re-organization [58]. We also discovered that APC targets and H3K4ME2 were associated with ARMC10. Adenomatous polyposis coli (APC) gene has been previously found to have a Wnt/β-catenin dependent effect on tumorigenesis and could regulate cell proliferation and migration via activating long non-coding RNA [59–61]. Lysine-specific demethylase 1 (LSD1), a chromatin regulator and its target H3K4ME2 often increased and contributed to cell proliferation, migration and apoptosis inhibition in cancer [62,63]. Moreover, we constructed the PPI network and discovered multiple pathways and biological processes related to those hub genes. But their relationship with ARMC10 was firstly been put forward and the precise mechanism needed further exploration.

Tumor microenvironment has been brought into focus in the progression of cancer for a long time, especially immune infiltrates [64]. Tumor-infiltrating immune cells (TIICs) have close connection with prognosis in various cancers [65,66]. In our study, we found the relevance between ARMC10 expression and several clinicopathological factors in PAAD patients, including higher clinical T/M stage, higher pathologic stage, R1&R2 residual tumor, histologic grade G3/G4. In addition, we detected that ARMC10 expression was positively relevant to the infiltration of Th2 cells, T helper cells and negatively relevant to pDC cells infiltration, indicating that ARMC10 may be a prognostic biomarker of PAAD concerning with immune infiltration. Pancreatic cancer is characterized by a marked desmoplasia with a predominant Th2 over Th1 lymphoid infiltration [67]. Previous study showed that different immune subtype in tumor microenvironment had different prognosis and the enrichment of Th2 cells in PDAC was significantly associated with disease risk [68]. It might relate to Th2-type inflammation through thymic stromal lymphopoietin-dependent induction [67]. In PAAD, brain-derived neurotrophic factor could modulate Th2 cells migration through related chemokine/chemokine receptors, which was correlated with chemotherapeutics sensitivity and immune checkpoints expression [69]. Dendritic cells play an important role in antitumor immunity [70]. pDC could secrete type I IFN, present antigen to naïve T cells and so was related to cancer immunology [71–73]. Current trials have shown that pDCs could generate anti-tumor CD8 T cell immunity and had a suppressive role in tumor progression [74]. The neoantigen-induced tumor progression in PAAD due to pathogenic Th17 response was associated with infiltrating conventional DCs (cDCs) and cDC function restoration had multiple roles in different stage of PAAD [75]. Thus, it has been an important target to improve cancer immunotherapy [76]. It can be inferred that pDC in highly expressed ARMC10 patients may affect antigen-specific immunity and mediate tumor progression. As for the clinical factors, ARMC10 was shown to be an independent prognostic indicator of poor OS, DSS and PFI in PAAD patients. The constructed nomogram showed a great prediction of 1-, 3-, 5- year survival with the C-index of 0.727 (95%CI: 0.696–0.758). Then, the influence of ARMC10 on PAAD cell proliferation, invasion and migration was examined in vitro. We discovered that ARMC10 suppression could alleviate malignant phenotype of PAAD, indicating the probability of ARMC10 to be the potential therapeutic target. The critical role of immune infiltration and ARMC10 in PAAD needs further explorations.

There still exists some limitations in our study. The clinical factors involved in our prediction model are not comprehensive enough. But as our data was acquired from public databases, the missing of some clinical factors was inevitable due to the heterogeneity of different clinical centers. Because of the restricted condition, the relevance between ARMC10 expression and PAAD prognosis was failed to be verified in another large cohort. In addition, subject to the analytical methods, the associated functions and pathways must not be limited to the results in our study. Our research is a pilot study, and the concrete molecular mechanism and clinical application need further in-depth studies afterwards. In addition, we compared the ARMC10 expression in the total tumor tissues, which may be confounded by tumor cellularity.

So, the exploitable role of ARMC10 in PAAD and underlying mechanisms need more studies in depth.

5. Conclusion

Collectively, we put forward the prognostic value of ARMC10 in PAAD patients with regard to glutamate receptor, cation channels, histone modification and immune infiltration, etc. We also revealed the association between ARMC10 and clinicopathological significance in PAAD, indicating ARMC10 may be an exploitable therapeutic target.

Availability of data and materials

The data generated or used in this study were available in the article/Supplementary materials. Requests could be made to corresponding author directly.

Author contributions

Tianhao Li: Conceptualization (equal); Data curation (equal); Formal analysis (equal); Methodology (equal); Software (equal); Writing-original draft (equal); Writing-review & editing (equal). **Xiaohan Qin:** Conceptualization (equal); Data curation (equal); Investigation (equal); Methodology (equal); Visualization (equal); Writing-original draft (equal); Writing-review & editing (equal). **Liquan Wang:** Conceptualization (equal); Data curation (equal); Writing-original draft (equal); Writing-review & editing (equal). **Cheng Qin and Bangbo Zhao:** Formal analysis (equal); Visualization (equal); Writing original draft (equal); Writing-review & editing (equal). **Hongtao Cao:** Conceptualization (equal); Data curation (equal); Formal analysis (equal); Resources (equal); Software (equal). **Xiaoying Yang:** Conceptualization (equal); Data curation (equal); Visualization (equal). **Yuanyang Wang:** Conceptualization (equal); Data curation (equal); Visualization (equal); Writing-review & editing (equal). **Zeru Li:** Data curation (equal); Formal analysis (equal); Software (equal); Visualization (equal). **Xingtong Zhou:** Conceptualization (equal); Software (equal); Writing-review & editing (equal). **Weibin Wang:** Conceptualization (equal); Data curation (equal); Formal analysis (equal); Funding acquisition (equal); Investigation (equal); Project administration (equal); Supervision (equal).

Ethics approval and consent to participate

Not applicable.

Consent for publication

All authors consent to the publication of this article.

Declaration of competing interest

The authors declare that they have no known competing financial interests or personal relationships that could have appeared to influence the work reported in this paper.

Abbreviations

ARMC10   Armadillo repeat-containing 10
PAAD   Pancreatic adenocarcinoma
TCGA   The Cancer Genome Atlas
GEO   gene expression omnibus

OS   Overall-Survival
DSS   Disease-Specific Survival
PFI   Progression-Free Interval
ARMCX/ALEX Armadillo repeat-containing X-linked protein
PPI   protein-protein interaction
DEGs   differentially expressed genes
KM   Kaplan-Meier
GO   gene ontology
KEGG   Kyoto Encyclopedia of Genes and Genomes
GSEA   gene set enrichment analysis
ssGSEA   single sample gene set enrichment analysis
TPM   Transcripts Per Million
ROC   Receiver operating characteristic
FC   fold change
WB   western blotting
SDS-PAGE   Sodium Dodecyl Sulfate-Polyacrylamide Gel Electrophoresis
CCK-8   Cell Counting Kit-8
GTEx   Genotype-Tissue Expression
ACC   adrenocortical carcinoma
BLCA   bladder urothelial carcinoma
BRCA   breast filtrating carcinoma
CHOL   cholangiocarcinoma
COAD   colon adenocarcinoma
DLBCL   diffuse large B cell lymphoma
ESCA   esophageal carcinoma
GBM   pleomorphic glioma
HNSC   Head and Neck squamous cell carcinoma
KIRC   renal clear cell carcinoma
KIRP   renal papillary cell carcinoma
LGG   brain low grade glioma
LIHC   liver hepatocellular carcinoma
LUAD   lung adenocarcinoma
LUSC   lung squamous cell carcinoma
OV   ovarian serous cystadenocarcinoma
PRAD   prostate cancer
READ   rectum adenocarcinoma
SKCM   skin melanoma
STAD   gastric cancer
TGCT   testicular germ cell tumors
THCA   thyroid cancer
THYM   thymic cancer
UCEC   endometrial cancer
LAML   acute myeloid leukemia
AUC   area under the curve
BPs   Biological Processes
CCs   Cellular Components
MFs   Molecular Functions
MSigDB   the Molecular Signatures Database
NES   normalized enrichment score
HCP   high-CpG-density promoters
H3K4me2   histone H3 dimethylation mark at K4
NPC   neural precursor cells
Th2 cell   T helper 2 cells
pDCs   plasmacytoid dendritic cells
CREB   cAMP-response element binding protein
TRPV4   transient receptor potential cation channel subfamily V member 4
TRPM7/8   transient receptor potential cation channel subfamily M member 7/8
TPC2   two-pore channel 2
TNBC   triple-negative breast cancer
TRAIL   tumor necrosis factor-related apoptosis-inducing ligand
KCMF1   Potassium channel modulatory factor 1

APC   Adenomatous polyposis coli
LSD1   Lysine-specific demethylase 1
TIICs   Tumor-infiltrating immune cells
cDCs   conventional dendritic cells

Appendix A. Supplementary data

Supplementary data to this article can be found online at https://doi.org/10.1016/j.heliyon.2023.e20464.

References

[1] R.L. Siegel, et al., Cancer statistics, Ca - Cancer J. Clin. 72 (1) (2022) 7–33, 2022.
[2] X. Geng, et al., Tumor cell derived lnc-FSD2-31:1 contributes to cancer-associated fibroblasts activation in pancreatic ductal adenocarcinoma progression through extracellular vesicles cargo MiR-4736, Adv. Sci. 10 (10) (2023), e2203324.
[3] M.P. Kim, et al., Oncogenic KRAS recruits an expansive transcriptional network through mutant p53 to drive pancreatic cancer metastasis, Cancer Discov. 11 (8) (2021) 2094–2111.
[4] T. Kamisawa, et al., Pancreatic cancer, Lancet 388 (10039) (2016) 73–85.
[5] G.M. Heestand, J.D. Murphy, A.M. Lowy, Approach to patients with pancreatic cancer without detectable metastases, J. Clin. Oncol. 33 (16) (2015) 1770–1778.
[6] H. Borchardt, et al., miR24-3p activity after delivery into pancreatic carcinoma cell lines exerts profound tumor-inhibitory effects through distinct pathways of apoptosis and autophagy induction, Cancer Lett. 503 (2021) 174–184.
[7] A.Z. Daoud, et al., MicroRNAs in Pancreatic Cancer: biomarkers, prognostic, and therapeutic modulators, BMC Cancer 19 (1) (2019) 1130.
[8] Z. Xu, et al., MicroRNA-505, suppressed by oncogenic long non-coding RNA LINC01448, acts as a novel suppressor of glycolysis and tumor progression through inhibiting HK2 expression in pancreatic cancer, Front. Cell Dev. Biol. 8 (2020), 625056.
[9] C. Corradi, et al., Genome-wide scan of long noncoding RNA single nucleotide polymorphisms and pancreatic cancer susceptibility, Int. J. Cancer 148 (11) (2021) 2779–2788.
[10] J. Wang, et al., Long non-coding RNA H19, a novel therapeutic target for pancreatic cancer, Mol. Med. 26 (1) (2020) 30.
[11] Y. Wang, et al., Research progress on long non-coding RNAs and their roles as potential biomarkers for diagnosis and prognosis in pancreatic cancer, Cancer Cell Int. 20 (2020) 457.
[12] X. Han, et al., Upregulated circRNA hsa_circ_0071036 promotes tumourigenesis of pancreatic cancer by sponging miR-489 and predicts unfavorable characteristics and prognosis, Cell Cycle 20 (4) (2021) 369–382.
[13] C. Limb, et al., The role of circular RNAs in pancreatic ductal adenocarcinoma and biliary-tract cancers, Cancers 12 (11) (2020).
[14] X. Xiong, et al., Circular RNA CDR1as promotes tumor progression by regulating miR-432-5p/E2F3 axis in pancreatic cancer, Cancer Cell Int. 21 (1) (2021) 112.
[15] S. Chen, et al., CLK1/SRSF5 pathway induces aberrant exon skipping of METTL14 and Cyclin L2 and promotes growth and metastasis of pancreatic cancer, J. Hematol. Oncol. 14 (1) (2021) 60.
[16] M. Oshi, et al., Annexin A1 expression is associated with epithelial-mesenchymal transition (EMT), cell proliferation, prognosis, and drug response in pancreatic cancer, Cells 10 (3) (2021).
[17] H. Zhu, et al., PARP inhibitors in pancreatic cancer: molecular mechanisms and clinical applications, Mol. Cancer 19 (1) (2020) 49.
[18] R. Serrat, et al., The Armc10/SVH gene: genome context, regulation of mitochondrial dynamics and protection against Aβ-induced mitochondrial fragmentation, Cell Death Dis. 5 (4) (2014) e1163.
[19] G. López-Doménech, et al., The Eutherian Armcx genes regulate mitochondrial trafficking in neurons and interact with Miro and Trak2, Nat. Commun. 3 (2012) 814.
[20] T. Wang, et al., ARMCX family gene expression analysis and potential prognostic biomarkers for prediction of clinical outcome in patients with gastric carcinoma, BioMed Res. Int. 2020 (2020), 3575038.
[21] J. Du, et al., Alex3 suppresses non-small cell lung cancer invasion via AKT/Slug/E-cadherin pathway, Tumour Biol 39 (7) (2017), 1010428317701441.
[22] H. Iseki, et al., ALEX1 suppresses colony formation ability of human colorectal carcinoma cell lines, Cancer Sci. 103 (7) (2012) 1267–1271.
[23] I.V. Kurochkin, et al., ALEX1, a novel human armadillo repeat protein that is expressed differentially in normal tissues and carcinomas, Biochem. Biophys. Res. Commun. 280 (1) (2001) 340–347.
[24] Y. Kusama, et al., Expression and tissue distribution of human X-linked armadillo repeat containing-6, Exp. Ther. Med. 1 (2) (2010) 395–399.
[25] S. Mirra, et al., ARMCX3 mediates susceptibility to hepatic tumorigenesis promoted by dietary lipotoxicity, Cancers 13 (5) (2021).
[26] L. Badea, et al., Combined gene expression analysis of whole-tissue and microdissected pancreatic ductal adenocarcinoma identifies genes specifically overexpressed in tumor epithelia, Hepato-Gastroenterology 55 (88) (2008) 2016–2027.
[27] H. Pei, et al., FKBP51 affects cancer cell response to chemotherapy by negatively regulating Akt, Cancer Cell 16 (3) (2009) 259–266.
[28] N. Yu, et al., Wip1 regulates wound healing by affecting activities of keratinocytes and endothelial cells through ATM-p53 and mTOR signaling, Burns (2023).
[29] H.Q. Cai, et al., Identifying predictive gene expression and signature related to temozolomide sensitivity of glioblastomas, Front. Oncol. 10 (2020) 669.
[30] L. Szadai, et al., Deep proteomic analysis on biobanked paraffine-archived melanoma with prognostic/predictive biomarker read-out, Cancers 13 (23) (2021).
[31] Q. Huang, et al., Construction and comprehensive analysis of a novel prognostic signature associated with pyroptosis molecular subtypes in patients with pancreatic adenocarcinoma, Front. Immunol. 14 (2023), 1111494.
[32] Y. Ino, et al., Immune cell infiltration as an indicator of the immune microenvironment of pancreatic cancer, Br. J. Cancer 108 (4) (2013) 914–923.
[33] M. Hatzfeld, The armadillo family of structural proteins, Int. Rev. Cytol. 186 (1999) 179–224.
[34] B. Rubinfeld, et al., Binding of GSK3beta to the APC-beta-catenin complex and regulation of complex assembly, Science 272 (5264) (1996) 1023–1026.
[35] Z. Chen, et al., Global phosphoproteomic analysis reveals ARMC10 as an AMPK substrate that regulates mitochondrial dynamics, Nat. Commun. 10 (1) (2019) 104.
[36] H. Iseki, et al., Human Arm protein lost in epithelial cancers, on chromosome X 1 (ALEX1) gene is transcriptionally regulated by CREB and Wnt/beta-catenin signaling, Cancer Sci. 101 (6) (2010) 1361–1366.
[37] Z. Mou, A.R. Tapper, P.D. Gardner, The armadillo repeat-containing protein, ARMCX3, physically and functionally interacts with the developmental regulatory factor Sox10, J. Biol. Chem. 284 (20) (2009) 13629–13640.
[38] J. Turner, et al., Kinase gene fusions in defined subsets of melanoma, Pigment Cell Melanoma Res 30 (1) (2017) 53–62.
[39] E. Dornier, et al., Glutaminolysis drives membrane trafficking to promote invasiveness of breast cancer cells, Nat. Commun. 8 (1) (2017) 2255.
[40] R. Shah, S. Chen, Metabolic signaling cascades prompted by glutaminolysis in cancer, Cancers 12 (9) (2020).
[41] R. Shah, et al., Concurrent targeting of glutaminolysis and metabotropic glutamate receptor 1 (GRM1) reduces glutamate bioavailability in GRM1(+) melanoma, Cancer Res. 79 (8) (2019) 1799–1809.
[42] P. Zhang, et al., Genomic sequencing and editing revealed the GRM8 signaling pathway as potential therapeutic targets of squamous cell lung cancer, Cancer Lett. 442 (2019) 53–67.

[43] Z. Zhang, et al., Activation of type 4 metabotropic glutamate receptor promotes cell apoptosis and inhibits proliferation in bladder cancer, J. Cell. Physiol. 234 (3) (2019) 2741–2755.

[44] Z. Zhang, et al., Activity of metabotropic glutamate receptor 4 suppresses proliferation and promotes apoptosis with inhibition of gli-1 in human glioblastoma cells, Front. Neurosci. 12 (2018) 320.

[45] S. Ripka, et al., Glutamate receptor GRIA3–target of CUX1 and mediator of tumor progression in pancreatic cancer, Neoplasia 12 (8) (2010) 659–667.

[46] L. Xie, et al., At-labelled mGluR1 inhibitor induces cancer senescence to elicit long-lasting anti-tumor efficacy, Cell Rep Med (2023), 100960.

[47] K. Eddy, et al., Implications of a neuronal receptor family, metabotropic glutamate receptors, in cancer development and progression, Cells 11 (18) (2022).

[48] T. Huang, et al., Cannabidiol inhibits human glioma by induction of lethal mitophagy through activating TRPV4, Autophagy (2021) 1–15.

[49] X. Li, et al., Calcium and TRPV4 promote metastasis by regulating cytoskeleton through the RhoA/ROCK1 pathway in endometrial cancer, Cell Death Dis. 11 (11) (2020) 1009.

[50] X. Liu, et al., Activation of PTEN by inhibition of TRPV4 suppresses colon cancer development, Cell Death Dis. 10 (6) (2019) 460.

[51] Y. Huang, et al., Transient receptor potential melastin 8 (TRPM8) channel regulates proliferation and migration of breast cancer cells by activating the AMPK-ULK1 pathway to enhance basal autophagy, Front. Oncol. 10 (2020), 573127.

[52] S.J.P. Pratt, et al., Mechanoactivation of NOX2-generated ROS elicits persistent TRPM8 Ca(2+) signals that are inhibited by oncogenic KRas, Proc. Natl. Acad. Sci. U.S.A. 117 (42) (2020) 26008–26019.

[53] P. Rybarczyk, et al., Transient receptor potential melastin-related 7 channel is overexpressed in human pancreatic ductal adenocarcinomas and regulates human pancreatic cancer cell migration, Int. J. Cancer 131 (6) (2012) E851–E861.

[54] C. Song, et al., Suppression of TRPM7 enhances TRAIL-induced apoptosis in triple-negative breast cancer cells, J. Cell. Physiol. 235 (12) (2020) 10037–10050.

[55] A.S. Rosato, R. Tang, C. Grimm, Two-pore and TRPML cation channels: regulators of phagocytosis, autophagy and lysosomal exocytosis, Pharmacol. Ther. 220 (2021), 107713.

[56] M. Müller, et al., Gene editing and synthetically accessible inhibitors reveal role for TPC2 in HCC cell proliferation and tumor growth, Cell Chem. Biol. (2021).

[57] S. Beilke, et al., The zinc-finger protein KCMF1 is overexpressed during pancreatic cancer development and downregulation of KCMF1 inhibits pancreatic cancer development in mice, Oncogene 29 (28) (2010) 4058–4067.

[58] S. Manoli, et al., The activity of kv 11.1 potassium channel modulates F-actin organization during cell migration of pancreatic ductal adenocarcinoma cells, Cancers 11 (2) (2019).

[59] K.M. Alula, et al., Nuclear partitioning of Prohibitin 1 inhibits Wnt/β-catenin-dependent intestinal tumorigenesis, Oncogene 40 (2) (2021) 369–383.

[60] F.W. Wang, et al., APC-activated long noncoding RNA inhibits colorectal carcinoma pathogenesis through reduction of exosome production, J. Clin. Invest. 131 (7) (2021).

[61] X.Z. Yang, et al., LINC01133 as ceRNA inhibits gastric cancer progression by sponging miR-106a-3p to regulate APC expression and the Wnt/β-catenin pathway, Mol. Cancer 17 (1) (2018) 126.

[62] Y. Pan, et al., LINC00675 suppresses cell proliferation and migration via downregulating the H3K4me2 level at the SPRY4 promoter in gastric cancer, Mol. Ther. Nucleic Acids 22 (2020) 766–778.

[63] S. Wang, D.H. Meyer, B. Schumacher, H3K4me2 regulates the recovery of protein biosynthesis and homeostasis following DNA damage, Nat. Struct. Mol. Biol. 27 (12) (2020) 1165–1177.

[64] Y. Nie, et al., CXCL5 has potential to Be a marker for hepatocellular carcinoma prognosis and was correlating with immune infiltrates, Front. Oncol. 11 (2021), 637023.

[65] S. Liu, et al., Prognostic analysis of tumor mutation burden and immune infiltration in hepatocellular carcinoma based on TCGA data, Aging (Albany NY) 13 (8) (2021) 11257–11280.

[66] L. Ye, et al., Tumor-infiltrating immune cells act as a marker for prognosis in colorectal cancer, Front. Immunol. 10 (2019) 2368.

[67] L. De Monte, et al., Intratumor T helper type 2 cell infiltrate correlates with cancer-associated fibroblast thymic stromal lymphopoietin production and reduced survival in pancreatic cancer, J. Exp. Med. 208 (3) (2011) 469–478.

[68] X. Wang, et al., Reveal the heterogeneity in the tumor microenvironment of pancreatic cancer and analyze the differences in prognosis and immunotherapy responses of distinct immune subtypes, Front. Oncol. 12 (2022), 832715.

[69] Y. Zhu, et al., BDNF acts as a prognostic factor associated with tumor-infiltrating Th2 cells in pancreatic adenocarcinoma, Dis. Markers 2021 (2021), 7842035.

[70] I. Plesca, et al., Clinical significance of tumor-infiltrating conventional and plasmacytoid dendritic cells in pancreatic ductal adenocarcinoma, Cancers 14 (5) (2022).

[71] L. Chaperot, et al., Virus or TLR agonists induce TRAIL-mediated cytotoxic activity of plasmacytoid dendritic cells, J. Immunol. 176 (1) (2006) 248–255.

[72] T.W. Kim, et al., Transcriptional repression of IFN regulatory factor 7 by MYC is critical for type I IFN production in human plasmacytoid dendritic cells, J. Immunol. 197 (8) (2016) 3348–3359.

[73] J. Martinek, et al., Interplay between dendritic cells and cancer cells, Int Rev Cell Mol Biol 348 (2019) 179–215.

[74] C. Fu, et al., DC-based vaccines for cancer immunotherapy, Vaccines 8 (4) (2020). Basel.

[75] S. Hegde, et al., Dendritic cell paucity leads to dysfunctional immune surveillance in pancreatic cancer, Cancer Cell 37 (3) (2020) 289–307.e9.

[76] S.K. Wculek, et al., Dendritic cells in cancer immunology and immunotherapy, Nat. Rev. Immunol. 20 (1) (2020) 7–24.